Submitted to Engineering Structures

Seismic Response of Building Frames with Flexible Base Optimized for Reverse Rocking Response

Makoto Ohsaki[1*], Osamu Iwatsuki[1] and Hidekazu Watanabe[1**]
[1]Department of Architecture, Hiroshima University,
1-4-1, Kagamiyama, Higashi-Hiroshima 739-8527, Japan.

Abstract

A reverse rocking response is investigated for a steel frame that has flexible base. The mechanism of response reduction is first investigated using a simple flexible base model consisting of truss elements. It is demonstrated that the roof displacement is reduced by the dominant second mode, in which the base rotates in the opposite direction to the upper frame. Seismic responses of the frame can be further reduced by installing viscous dampers at the support. A topology optimization approach is next presented for design of flexible base structure consisting of frame elements. It is shown that the cross-sectional properties and nodal locations are successfully optimized using a nonlinear programming approach to generate a flexible base.

Keywords: Reverse rocking, Seismic response, Building frame, Flexible structure, Optimization

１． Introduction

The approaches to reduction of seismic responses of building frames are classified into (a) *seismic design*: stiff design of the structural members so as to resist the seismic load within the allowable small deformation, (b) *base isolation*: reduction of the seismic input energy by increasing the natural period, and (c) *passive vibration control*:

*Corresponding author: Department of Architecture, Hiroshima University, 1-4-1, Kagamiyama, Higashi-Hiroshima 739-8527, Japan. E-mail: ohsaki@hiroshima-u.ac.jp. Phone: +81-82-424-7794

**Present address: Materials and Structures Laboratories, Tokyo Institute of Technology, 4259, Nagatsuda, Midori, Yokohama 226-8503, Japan.

dissipation of seismic energy utilizing plastic deformation, viscosity, and/or inertia. In this paper, we present a new approach that is not categorized into any of the above three approaches.

The basic principle of seismic design of a building frame does not allow uplift of the column-base, because it may lead to a damage to the foundation as well as an unexpectedly large deformation of the frame during a severe earthquake. However, it is possible to utilize a rocking system, allowing uplift of the column base, to reduce deformation of the upper frame through energy dissipation at the column base as well as the increase of potential energy of the upper frame due to overturning moment [1-7]. A rocking system also reduces the input energy by increasing the natural period of the frame during uplift. Seismic responses can also be reduced utilizing a soft first story [8, 9], partial uplift of each column base [10], and base isolation with rocking device [11].

On the other hand, a flexible structure such as a compliant mechanism [12-14], which utilizes flexibility of structural elements, can also be used for devices for seismic response reduction such as base isolation [15, 16] and tuned mass damper [17, 18]. A flexible structure enables large deformation and stores elastic strain energy through deformation.

Optimization of frames and trusses under seismic excitation has been extensively studied since 1970s. In the early stage, the responses were evaluated using a response spectrum approach [19, 20]. If a single mode dominates in the seismic response, then reduction of seismic response is closely related to mode control. In the field of mechanical engineering, several optimization approaches have been developed for specifying the mode shape [21, 22].

Recently, large deformation under long-period ground motion has become a critical issue for design of building frames. It is not always safe to utilize a base-isolation system, because it increases the first natural period and the structure may have large deformation under long-period motion. Therefore, a new seismic design approach that does not rely on increase of natural period is desired to be investigated.

Reduction of roof displacement and acceleration is important to mitigate damage of nonstructutal components and to improve serviceability in upper stories of a building frame during earthquake. Todorovska [23] proposed a rocking system with inclined rubber bearing. Zhang [24, 25] investigated a simple base model with inclined columns.

However, in these papers, the parameters such as the nodal locations and cross-sectional properties are not optimized, and the relation between stiffnesses of the upper and base structures are not discussed in detail. Rocking mechanisms can also be used for bridge piers [26, 27].

In this paper, we first investigate a reverse rocking response of a steel frame that has a flexible base. The mechanism of response reduction is investigated using a simple flexible base model consisting of truss elements. We next propose a new flexible structure that can reduce the roof displacement of a building frame utilizing rocking response. Topology optimization is carried out for a base model consisting of frame elements. It is shown that the cross-sectional properties and nodal locations are successfully optimized to generate a flexible base using a nonlinear programming approach.

2. Overview of flexible base for reverse rocking of building frame

We first demonstrate the effectiveness of reverse rocking response for reduction of roof displacement using a simple flexible base model as shown in Fig. 1, which is to be attached below the ground level of a plane frame. This structure can also be regarded as a soft first story. However, for the consistency of notation throughout the paper, we call this *flexible base*, and the beam between nodes 5 and 6 at the ground level is called *base beam*.

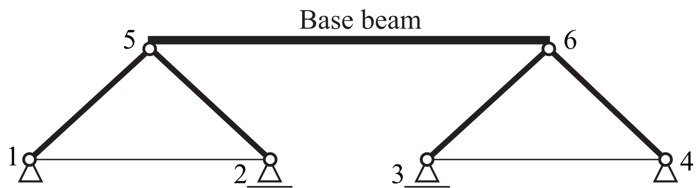

Fig. 1. A simple flexible base model.

Figure 2 illustrates the deformation of the base and upper frame subjected to horizontal loads, where the frame is simply represented by a column. Owing to the flexibility of the base, the frame with flexible base has a *reverse rocking response* as shown in Fig. 2(a); i.e., the base beam rotates in the opposite direction to the drift of frame to reduce the displacement of the roof. By contrast, if the frame has a stiff base, the base beam rotates slightly in the same direction as the frame as shown in Fig. 2(b).

This way, the roof displacement against horizontal loads can be reduced utilizing a flexible base.

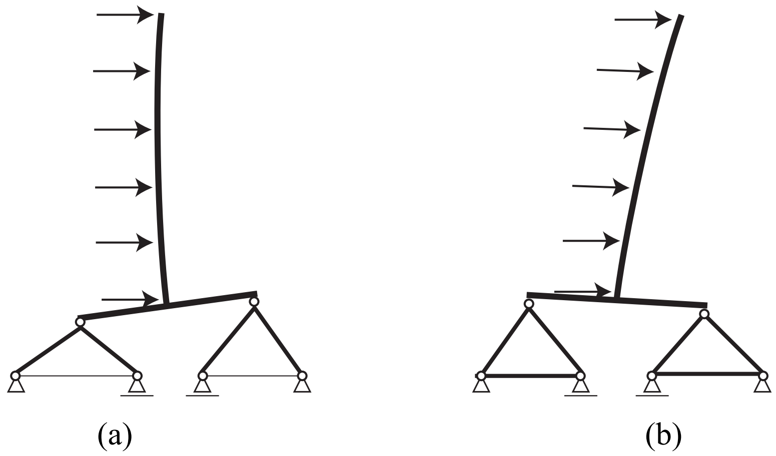

Fig. 2. Deformation of a frame model subjected to horizontal loads: (a) flexible base, (b) stiff base.

In the following, each member is indicated by the two nodes at its two ends; e.g., the member connecting nodes 1 and 2 is denoted by 'member 1-2'. The flexible base in Fig. 1 consists of six truss members and one stiff base beam (member 5-6). The truss members 1-5, 2-5, 3-6, and 4-6 are stiff enough, and horizontal truss members 1-2 and 3-4, which are called *thin members*, have small stiffness to realize a flexible base. Note that a thin member can actually be manufactured as a spring. The horizontal vibration of the upper frame leads to horizontal displacement of the roller supports 2 and 3; hence, the shape of dominant mode against horizontal excitation becomes different from that of the conventional model with a stiff base.

3. Design response spectrum and method of seismic response evaluation

The design acceleration response spectrum is specified according to the Notification 1461 of Ministry of Land, Infrastructure, Transport, and Tourism (MLIT), Japan, corresponding to the performance level of operational limit for the Design Based on Calculation of Response and Limit State, which is similar to the capacity spectrum approach. The amplification factor for the ground of second rank in Notification 1457 of MLIT is used. The response acceleration spectra for the damping factor $h = 0.02$, 0.05, and 0.10 are plotted in Fig. 3.

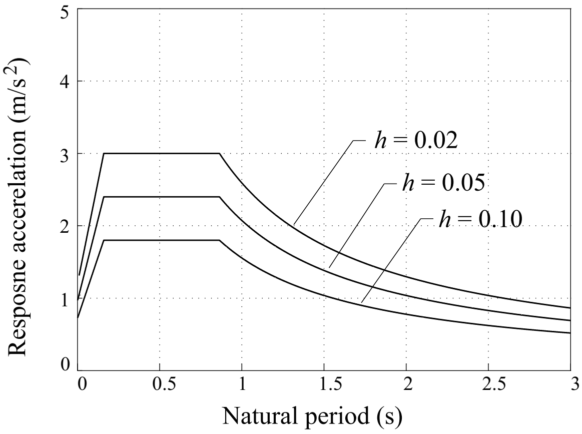

Fig. 3. Design acceleration response spectra for damping factors 0.02, 0.05, and 0.10.

In the following examples of a frame supported by the truss model in Secs. 4.2 and 4.3 and optimization process of the frame model in Sec. 5, the mean-maximum displacements against seismic excitations are evaluated using the square-root-of-sum-of-squares (SRSS) method. The pseudo-displacement response spectrum $S_{\mathrm{D}i} = S_{\mathrm{D}}(T_i, h_i)$ corresponding to the period T_i and damping factor h_i of the ith mode is defined from the acceleration response spectrum $S_{\mathrm{A}}(T_i, h_i)$ as $S_{\mathrm{D}i} = S_{\mathrm{A}}(T_i, h_i) / \left(\omega_i\right)^2$, where ω_i is the ith natural circular frequency. The mean-maximum response u_j of the jth displacement component is evaluated by

$$u_j = \sqrt{\sum_{i=1}^{s} \left(\beta_i \phi_j^i S_{\mathrm{D}i}\right)^2} \tag{1}$$

where β_i is the ith participation factor, ϕ_j^i is the jth component of the ith mode, and the lowest s modes are incorporated for response evaluation. Note that geometrical nonlinearity is not considered, because rotations of the base and upper frame are sufficiently small.

Ten ground motions compatible to the design acceleration response spectrum are generated for investigation of time-history responses. The duration of each motion is 20 sec., and the time increment is 0.01 sec. A standard approach of superposition of sinusoidal waves is used [28,29]. The phase of each discretized frequency component is defined using the phase spectrum of the El Centro EW ground motion, because it is important to use the sequence of phases of a recorded ground motion rather than generating it randomly [30]. Suppose the seismic ground motion is generated using K sinusoidal waves. The phase φ_i the ith frequency component is equal to φ_{i+J} of the El Centro wave, where $i+J \rightarrow i+j-K$ if $i+J>K$, and J is given randomly to generate ten different motions.

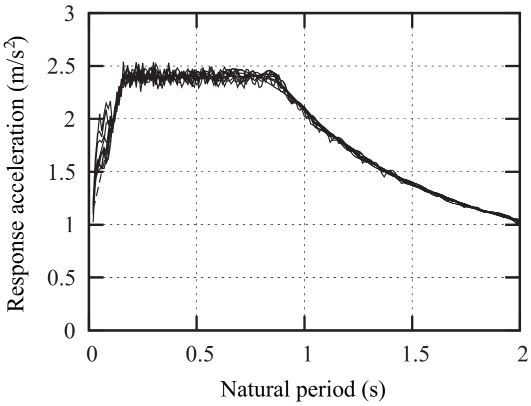

Fig. 4. Response spectra of ten artificial seismic ground motions compatible to design acceleration response spectrum with h = 0.05.

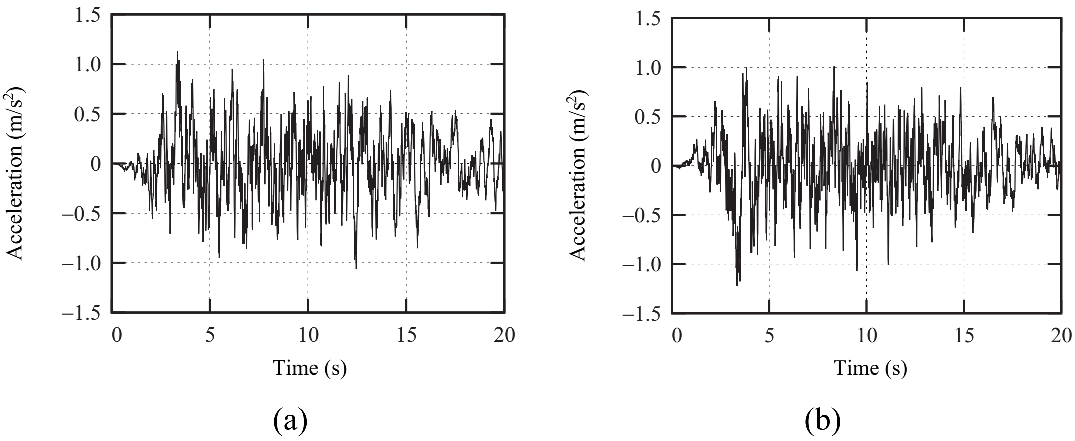

Fig. 5. Two examples of ground accelerations among ten artificial seismic ground motions.

Figure 4 shows response spectra of ten artificial seismic ground motions compatible to design acceleration response spectrum with h = 0.05. As seen from the figure, all ten seismic motions have good compatibility with the design response spectrum. Time histories of acceleration of two seismic motions are plotted in Fig. 5.

4 Simple frame model with flexible base

4.1 Frame model

Seismic responses are evaluated for the four-story plane frame as shown in Fig. 6 to investigate the effectiveness of utilizing flexibility of base for reduction of roof displacement. The span L is 10 m and the height H of each story is 3.5 m.

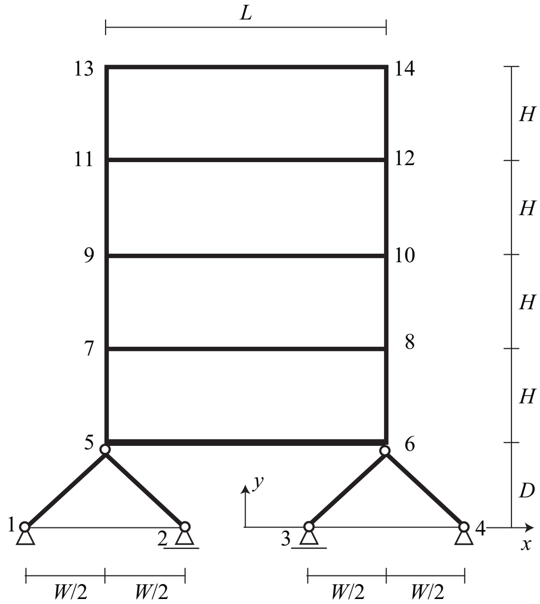

Fig. 6. A four-story plane frame with simple flexible base.

Throughout the paper, the material of frame and truss members is steel with Young's modulus 2.00×10^5 N/mm^2. The base beam between nodes 5 and 6 is assumed to be sufficiently stiff; i.e., large values 0.05 m^2 and 0.001 m^4 are assigned for the cross-sectional area A and second moment of area I, respectively. Cross-sectional areas and second moment of areas of other beams and columns are listed in Table 1. The mass of 5000 kg is attached at each node of the frame except nodes 5 and 6 that have 25000 kg to represent large mass at the ground level.

Table 1. Cross-sectional areas and second moment of areas of beams and columns of the upper frame.

	Cross-sectional area A (m^2)	Second moment of area I (m^4)
Beam	0.01332	0.000758
Column	0.02006	0.000358

The height D and width W of the base are 3.0 m and 6.0 m, respectively. The cross-sectional areas are 0.02 m^2 for stiff truss members 1-5, 2-5, 3-6, and 4-6. The cross-sectional area A_T of the thin members 1-2 and 3-4 is chosen as the parameter. The *stiff-model* is defined by A_T = 0.02 m^2. Note that the responses are almost the same when A_T is greater than 0.02 m^2.

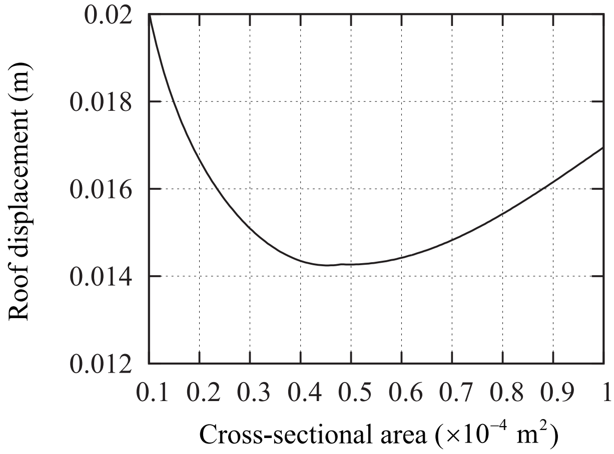

Fig.7. Relation between cross-sectional area A_T of thin members and roof displacement.

4.2 Modal response of flexible frame model

Seismic responses are evaluated using the SRSS method, where the lowest three modes are used with $h_i = 0.02$ for all modes for simplicity, because the contribution of the third mode is very small. The open-source frame analysis software OpenSees [31] is used for eigenvalue analysis.

The roof displacement is plotted in Fig. 7 with respect to the cross-sectional area A_T of the thin members. The roof displacement has the smallest value 0.01425 m at A_T = 0.4550 $\times 10^{-4}$ m^2, which is called *flexible-model*. By contrast, the roof displacement of stiff-model with A_T = 0.02 m^2 is 0.02553 m. The modal characteristics of the flexible and stiff models are listed in Tables 2(a) and (b), respectively.

Table 2. Modal characteristics of flexible and stiff models.

(a) Flexible-model

Mode	Period T_i (s)	Participation factor β_i	Effective mass ratio (%)
1st	0.8525	22.01	0.5383
2nd	0.4166	233.4	60.53
3rd	0.1528	28.16	0.8811

(b) Stiff-model

Mode	Period T_i (s)	Participation factor β_i	Effective mass ratio (%)
1st	0.5149	186.3	38.56
2nd	0.1578	67.65	5.085
3rd	0.08464	40.73	1.843

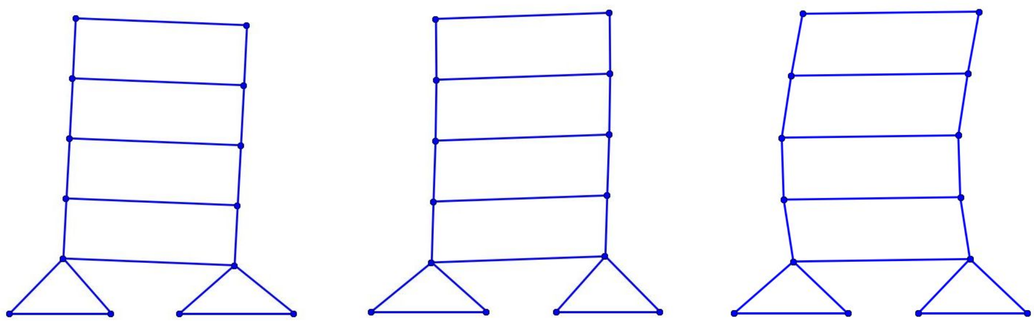

(a) 1st mode (b) 2nd mode (c) 3rd mode

Fig. 8. Three lowest modes of flexible-model.

As seen in Table 2, the effective mass ratios and participation factors of the 1st and 3rd modes decrease and those of the 2nd mode increase as a result of reducing the stiffness of the horizontal members 1-2 and 3-4. Fig. 8 shows the three lowest modes of the flexible-model. As seen from Fig. 8(b), the dominant 2nd mode has a rocking vibration of the base in the opposite direction to the drift of upper frame. Note that a higher mode with large displacements of nodes 5 and 6 has a large participation factor and effective mass ratio. However, the response corresponding to such mode is negligibly small, because its natural period is small, and accordingly, the pseudo-displacement response spectrum has a small value.

4.3 Time-history analysis

The frame analysis software OpenSees is also used for time-history response analysis. The damping matrix is defined by the Rayleigh damping with $h_i = 0.02$ for the 1st and 2nd modes.

Table 3 shows the mean-maximum responses of the stiff and flexible models under ten artificial seismic ground motions described in Sec. 3, which are compatible to the acceleration response spectrum in Fig. 3 with $h = 0.05$. The responses δ and a are the horizontal displacement and acceleration of the roof node 13, drift angle θ is the relative horizontal displacement between nodes 5 and 13 divided by the height 14 m of the frame, rocking angle ϕ is the relative vertical displacement between nodes 5 and 6 divided by the span 10 m, N is the axial force of the column member 6-8 of the 1st story, and b is the horizontal displacement of roller support 2. Note that θ and ϕ have positive values when they correspond to clockwise rotation.

As seen from the table, the maximum roof displacement of the flexible-model is 66.43% of the stiff-model. The rocking angle is more than 47 times as large as that of the stiff-model. The roof acceleration and the axial force of column in the 1st story are also reduced. The support displacement, which corresponds to the extension of the flexible members 1-2 and 3-4, is enhanced due to flexibility. Note that the strains of thick members 1-5, 2-5, 3-6, and 4-6 are less than 0.0001 for all seismic motions. The flexible-model-2 in the 3rd row of Table 3 is defined later.

Table 3. Mean values of maximum responses obtained by time-history analysis of frames subjected to ten spectrum-compatible ground motions; Flex/Stiff and Flex2/Stiff, respectively, denote the ratios of responses of flex-model and flex-model-2 to those of stiff-base.

	Roof disp. δ (cm)	Roof acc. a (m/s^2)	Drift angle θ (rad)	Rocking angle ϕ (rad)	Axial force N (kN)	Support disp. b (cm)
Stiff	2.711	4.414	1.934×10^{-3}	3.514×10^{-5}	93.17	0.006146
Flex (Flex/Stiff)	1.801 (0.6643)	3.615 (0.8190)	9.935×10^{-4} (0.5137)	1.664×10^{-3} (47.35)	70.10 (0.7523)	0.01542 (2.509)
Flex2 (Flex2/Stiff)	1.048 (0.3865)	2.172 (0.4923)	6.469×10^{-4} (0.3345)	7.469×10^{-4} (21.26)	42.11 (0.4520)	0.006562 (1.068)

The trajectory of rocking angle ϕ and the net drift angle $\theta - \phi$ is plotted in Figs. 9(a) and (b), respectively, for flexible and stiff models subjected to the seismic ground motion in Fig. 5(b). It is seen from Fig. 9(a) that the base and frame of the flexible-model rotate in the opposite directions and the response is reduced owing to the reverse rocking deformation. This plot also ensures that the 2nd mode in Fig. 8(b) dominates throughout the period of vibration. By contrast, Fig. 9(b) confirms that θ and ϕ of the stiff model have the same sign throughout the period of vibration. Note that the scales of axes, especially horizontal axis, are different in Figs. 9(a) and (b), because the rocking angle of stiff-model is very small.

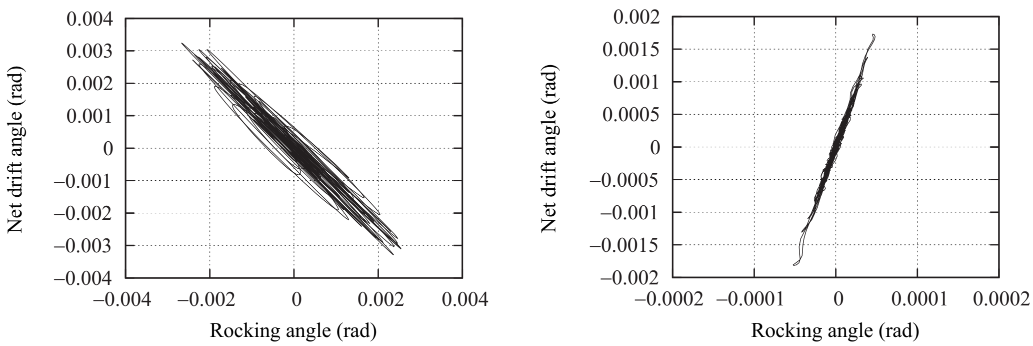

(a) (b)

Fig. 9. Trajectories of rocking angle and net drift angle of the frames subjected to the seismic motion in Fig. 5(b); (a) flexible-model, (b) stiff-model.

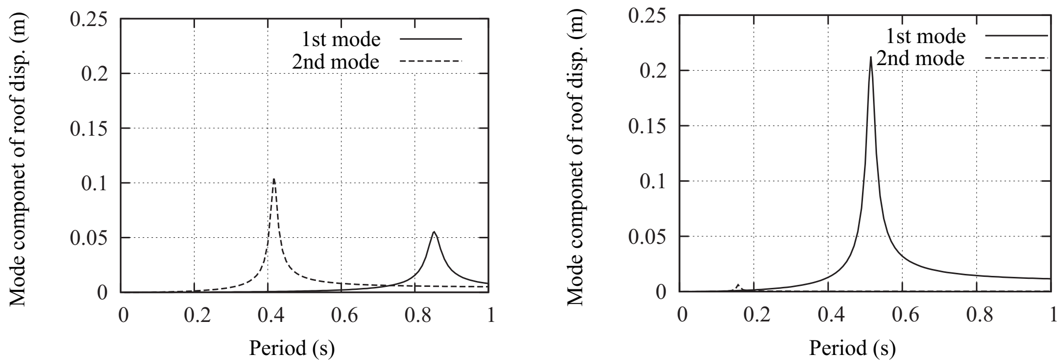

(a) (b)

Fig. 10. Maximum modal components of roof displacement with respect to the period of sinusoidal input of unit acceleration amplitude; solid line: 1st mode, dashed line: 2nd mode, (a) flexible-model, (b) stiff-model.

Figures 10(a) and (b) show the maximum modal components of roof displacement with respect to the period of sinusoidal input of unit acceleration amplitude (1.0 m/s^2) for flexible and stiff models, respectively. It can be confirmed from these figures that the 2nd mode dominates over the 1st mode in the flexible-model, while the 1st mode dominates in the stiff-model. Note that the 2nd mode of stiff-model in Fig. 10(b) is almost invisible.

The responses are further reduced by attaching viscous dampers along members 1-2 and 3-4. A parametric study is carried out for the damping coefficient C of the damper to find that the response has the smallest value for C = 500 kNs/m among the list {100, 200, …, 1000} (kNs/m). This model with damper is called *flexible-model-2*, for which the responses are listed in the 3rd row of Table 3. The roof displacement becomes 38.65% of the stiff-model by attaching the damper. The rocking angle is more than 21 times as large as that of the stiff-model, although it is about half of flexible-model without damper. The dampers reduce the horizontal displacement of node 2 to a small value that is almost the same as that of stiff-model.

Figures 11(a)-(c) show the time histories of roof displacement, drift angle, and rocking angle against the seismic ground motion in Fig. 5(b), where solid and dotted lines are the responses of flexible-model-2 with damper and stiff-model, respectively. As seen from Fig. 11(a), the roof displacement around 4 sec., when the stiff-model has the maximum value, is drastically reduced by reducing the stiffness of the base and installing viscous dampers. The drift angle is also reduced throughout the time history as shown in Fig. 11(b). By contrast, the rocking angle of base is enhanced, as shown in Fig. 11(c), by making the base flexible. Note that the rocking angle of stiff-model is very small.

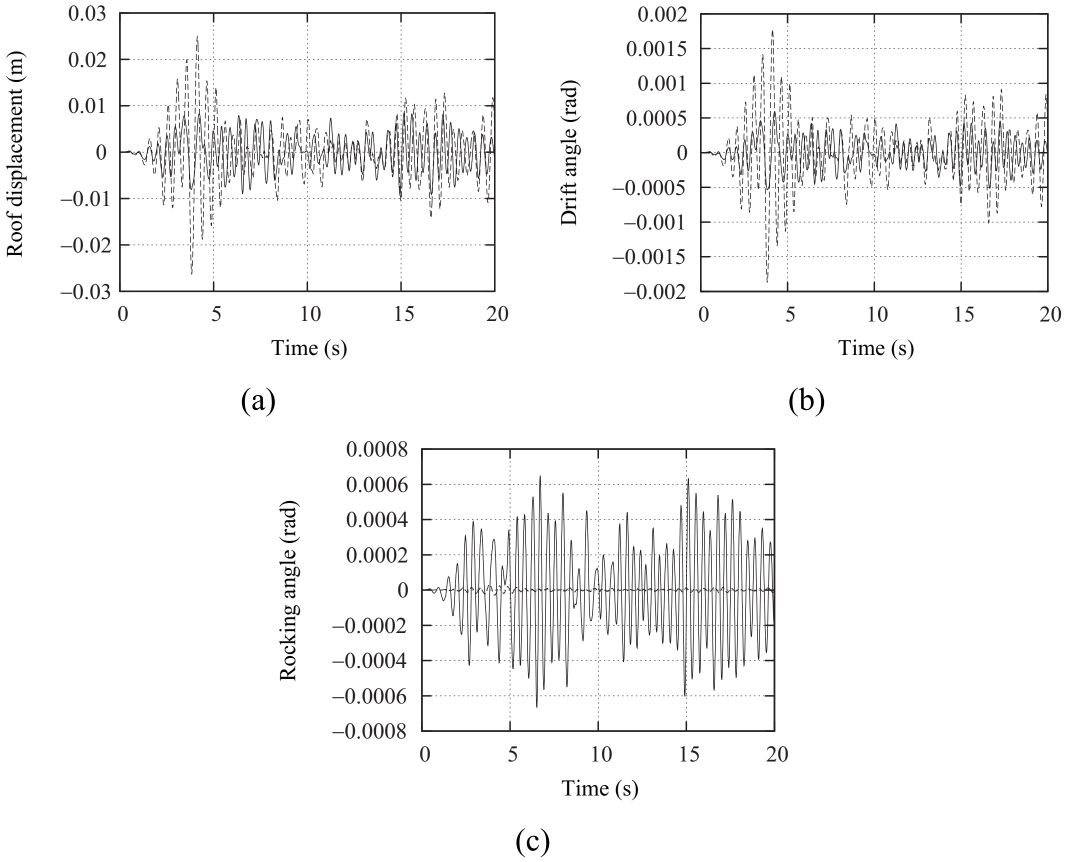

Fig. 11. Time histories of responses; (a): roof displacement, (b) drift angle between base and roof, (c) rocking angle of base; solid line: flexible-model-2, dotted line: stiff-model.

Figures 12(a)-(e) show the mean-maximum values of drift angle, net drift angle, shear force, floor displacement, and floor acceleration, respectively. The symbols '×', '□', and '+' correspond to stiff-model, flexible-model, and flexible-model-2, respectively. As seen from Figs. 12(a) and (d), the stiff-model has the largest displacement in upper stories and drift angles in all stories among the three models. However, if the rocking angle is extracted to evaluate the net drift angle, the flexible-model without damper has the largest values in the lower stories as shown in Fig. 12(b), because the rocking angle is opposite to the drift angle. The story shear forces that are computed from the shear forces of columns are plotted in Fig. 12(c), which shows that the stiff-model and flexible-model have almost the same shear forces. It has also been noted in Table 3 that the flexibility of base does not have any effect on the axial force of columns. Therefore, the flexible-base does not lead to increase of the cost for foundation. We can see from

Fig. 12(e) that the acceleration at base increases due to flexibility of the base; however, the flexible-model has a rather uniform distribution of the floor accelerations than the stiff-model, e.g., the ratios of roof acceleration to base acceleration of the flexible and stiff models are 2.332 and 7.472, respectively. Therefore, the roof acceleration can also be reduced utilizing the reverse rocking response.

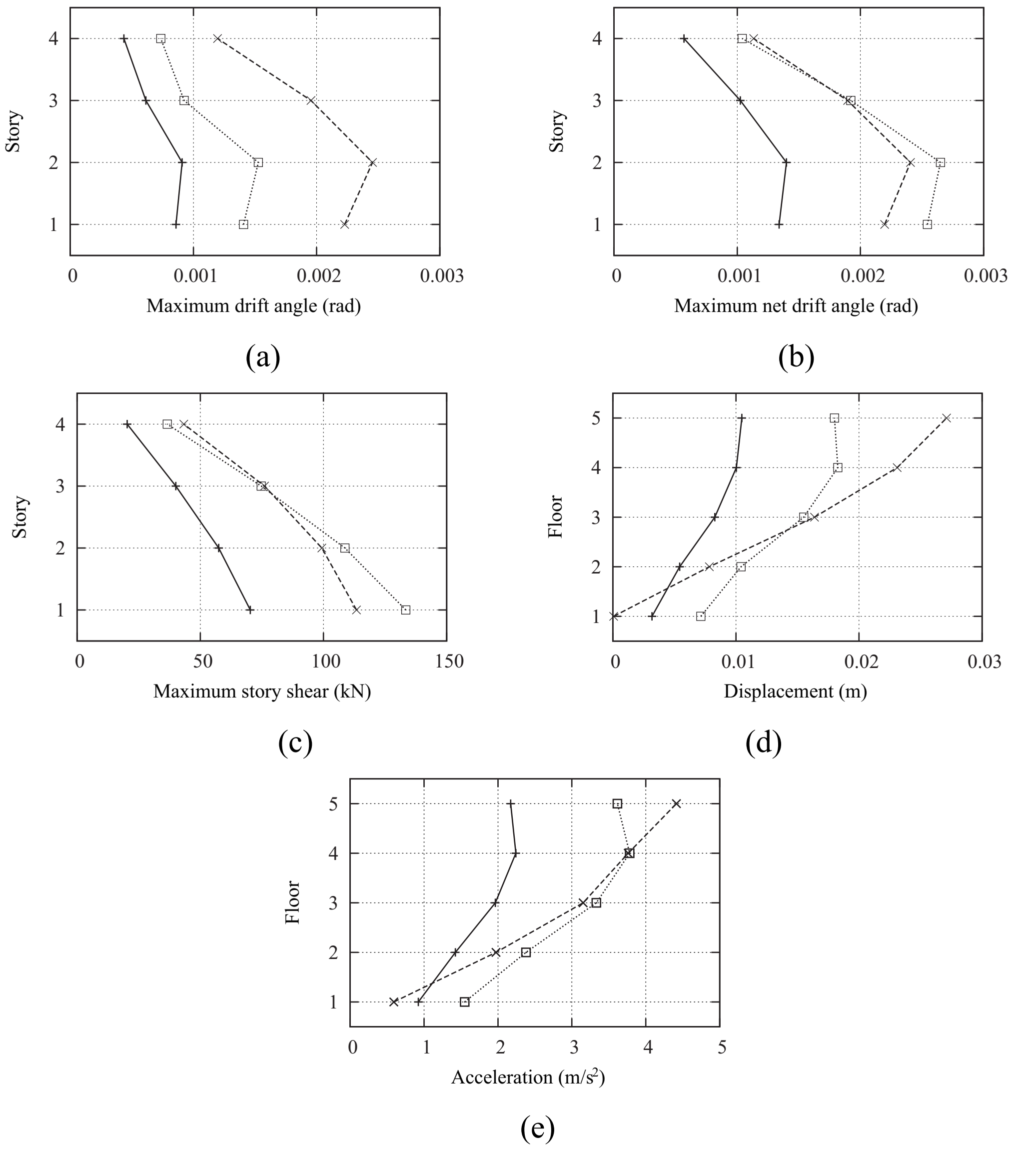

Fig. 12. Mean-maximum values of responses among ten waves; (a) drift angle, (b) net drift angle extracting rocking angle, (c) shear force, (d) floor displacement, (e) floor acceleration; dashed line with '×': stiff-model, dotted line with '□': flexible-model, solid line with '+': flexible-model-2.

4.4 Condition for reverse rocking response

A condition for generating rocking response of the base in the opposite direction to the drift of upper frame, which is simply called reverse rocking response, is investigated using the simple model as shown in Fig. 13, where M_0 and M_1, respectively, represent the mass of base and the concentrated mass of the remaining part of frame. We assume, for simplicity, that the frame moves rigidly against horizontal ground motion, and the load applied to the frame is supported by the external diagonal members 1-5 and 4-6, because the stiffnesses of members 1-2 and 3-4 are small enough so that the axial forces of members 2-5 and 3-6 are negligible.

Let a_0 and a_1 denote the *x*-directional accelerations applied at nodes 7 and 8, respectively. From the equilibrium in *x*-direction and the symmetry condition, the axial forces of members 1-5 and 4-6 are calculated as $(a_0 M_0 + a_1 M_1)/(2\cos\theta)$ and $-(a_0 M_0 + a_1 M_1)/(2\cos\theta)$, respectively. Then the moment due to these forces around node 7 is $[(a_0 M_0 + a_1 M_1) L \tan\theta]/2$, and counter-clockwise rocking occurs if the following condition is satisfied:

$$\frac{1}{2}(M_0 + \alpha M_1) L \tan\theta > \alpha M_1 H_1 \tag{2}$$

where $\alpha = a_1 / a_0$.

For the model in Fig. 6, H_1 is simply assigned as 7 m, which is a half of the height of the frame, and L = 10 m, $\theta = \pi/4$, $M_0 = 50000$ kg, $M_1 = 5000 \times 8 = 40000$ kg. Therefore, Eq. (2) reduces to $\alpha < 50/16 = 3.1250$. We can confirm from Fig. 12(e) that this condition is satisfied by the flexible-model.

Next, we investigate the dependency of the roof displacement of the frame in Fig. 6 on various properties of the frame. Optimal values of the cross-sectional area A_{T} of the thin member is found using the same procedure as Sec. 4.2., i.e., A_{T} is parametrically varied to find the minimum value of the roof displacement evaluated by the SRSS method.

Table 4 shows the optimal value of A_{T} and the corresponding roof displacements of flexible and stiff models for various values of span *L*, story height *H*, total mass M_0 at base, and width *W* of base. Note that the value of A_{T} for stiff model is 0.02 m^2. The standard parameter values L = 10 m, H = 3.5 m, M_0 = 50000 kg, and W = 6 m correspond to the model investigated in Sec. 4.2.

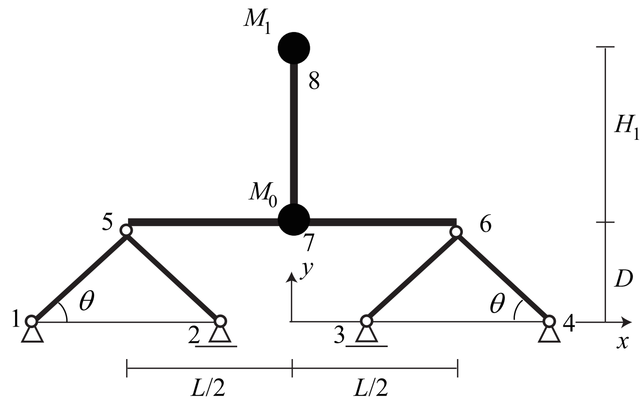

Fig. 13. A simple model for investigation of condition for reverse rocking response.

Table 4. Optimal cross-sectional areas and roof displacements of frames with flexible and stiff bases corresponding to various values of span L, story height H, total mass M_0 at base, and width W of base.

		Optimal cross-sectional area ($\times 10^{-4}$ m^2)	Roof disp. (m) of flexible model	Roof disp. (m) of stiff model	Flexible/Stiff
	8.0	0.17100	0.01616	0.02304	0.70121
	9.0	0.20700	0.01297	0.01724	0.75242
Span (m)	10.0	0.45500	0.01425	0.03498	0.40722
	11.0	0.67500	0.01506	0.04784	0.31469
	12.0	0.74400	0.01597	0.05598	0.28528
	3.00	1.14400	0.00998	0.05067	0.19687
	3.25	0.80400	0.01197	0.04384	0.27301
Story height (m)	3.50	0.45500	0.01425	0.03498	0.40722
	3.75	0.28500	0.01617	0.02548	0.63470
	4.00	0.13100	0.01845	0.01939	0.95145
	40000	0.19200	0.01502	0.01751	0.85755
	45000	0.33200	0.01456	0.02501	0.58213
Mass (kg)	50000	0.45500	0.01425	0.03498	0.40722
	55000	0.64300	0.01382	0.04477	0.30869
	60000	0.77400	0.01347	0.05569	0.24192
	3.0	0.26200	0.01304	0.02545	0.51252
	4.0	0.42400	0.01282	0.02543	0.50426
Width of base (m)	5.0	0.54000	0.01328	0.02546	0.52164
	6.0	0.45500	0.01425	0.02553	0.55813
	7.0	0.18800	0.01500	0.02563	0.58509

A small value of the ratio Flexible/Stiff indicates large reduction of roof displacement owing to the reverse rocking response. It is seen from Table 4 that larger span, smaller height, and larger base mass lead to enhancement of response reduction owing to reverse rockling response. Although the width of base does not have much effect on the response reduction property, a larger width leads to a larger roof displacement.

5. Optimization of frame structure for flexible base

In Sec. 4, we showed that the roof displacement can be reduced using a flexible base modeled as a truss structure. However, it is very difficult to construct the base using bars and pin joints, because a pin joint cannot rotate smoothly due to the friction corresponding to axial forces and deformation in the perpendicular direction to the plane. Therefore, in this section, we demonstrate that the flexible base in Fig. 1 can be naturally generated through optimization of a frame modeled by frame elements. The generalized ground structure approach to topology optimization of frame is used [32], where the unnecessary members are removed as a result of optimization from the highly connected ground structure. The nodal locations are also considered as variables.

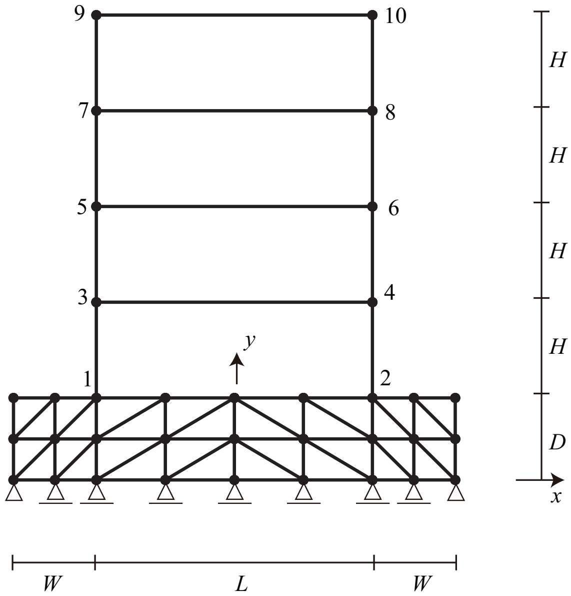

Fig. 14. A four-story plane frame with flexible base modeled by frame elements.

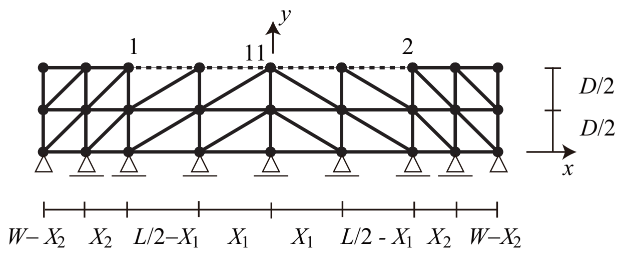

Fig. 15. Flexible base modeled by frame elements.

Consider a frame model as shown in Fig. 14, where L = 10 m, H = 3.5 m, D = 3 m, and W = 3 m. The properties of upper frame is the same as those of the frame in Fig. 6. The base in Fig. 15 consists of rigidly-jointed frame (beam-column) elements with square tube section as shown in Fig. 16 except the base beam indicated in dotted line, for which large values 0.05 m^2 and 0.001 m^4 are assigned for cross-sectional area and second moment of area, respectively. The ratio of t to B in Fig. 16 is fixed at 0.1, and the size B_i of the ith member in the base is considered as variable. The number of variables for the section is 28 considering symmetry of the base. The geometrical properties indicated by X_1 and X_2 in Fig. 15 are also considered as variables; i.e., the total number of variables is 30.

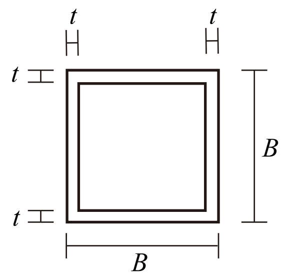

Fig. 16. Square tube section for members in the base.

The objective function to be minimized is the roof displacement δ evaluated using the SRSS method for the design acceleration spectrum in Fig. 3. Although other response quantities such as interstory drift angle and floor acceleration are important, the reverse rocking response should have most significance in reduction of overall deformation measured by the roof displacement. It has been confirmed in Table 3 and Fig. 12 that reverse rocking response does not have much negative effects on other response quantities.

The upper bound 1.0 s is given, as follows, for the 1st natural period to avoid response reduction owing to increase of natural period:

$$T_1 \leq 1.0 \tag{3}$$

Upper bound $D^{\mathrm{U}} = 0.0015$ m is assigned for the vertical (downward) displacements D_1 and D_{11} of nodes 1 and 11, respectively, under self-weight so that the base has enough vertical stiffness. Note that the mass of each member is assumed to be included in the concentrated nodal mass that is fixed.

It can be observed from the result of simple frame model in Sec. 4 that the absolute value of the participation factor for the 2nd mode should have sufficiently larger value than that of the 1st mode. Therefore, we assign the following constraint to enhance convergence to an optimal solution with flexible base:

$$|\beta_2| \geq 5|\beta_1| \tag{4}$$

The upper and lower bounds (m) for B_i are 0.35 and 0.01, respectively. The bounds are also given for X_1 and X_2. The design variables are denoted by vectors $\boldsymbol{B} = (B_1, \ldots, B_{28})$ and $\boldsymbol{X} = (X_1, X_2)$. Then, the optimization problem is formulated as

$$\begin{aligned}
&\text{Minimize} && \delta(\boldsymbol{B}, \boldsymbol{X}) \\
&\text{subject to} && T_1(\boldsymbol{B}, \boldsymbol{X}) \leq 1.0 \\
& && D_1(\boldsymbol{B}, \boldsymbol{X}) \leq 0.0015, \quad D_{11}(\boldsymbol{B}, \boldsymbol{X}) \leq 0.0015 \\
& && |\beta_2(\boldsymbol{B}, \boldsymbol{X})| \geq 5|\beta_1(\boldsymbol{B}, \boldsymbol{X})| \\
& && 0.01 \leq B_i \leq 0.35, \quad (i = 1, \ldots, 28) \\
& && 2.0 \leq X_1 \leq 3.0, \quad 1.0 \leq X_2 \leq 2.0
\end{aligned} \tag{5}$$

The optimization problem is solved using the optimization library SNOPT Ver. 7 [33], which utilizes sequential quadratic programming that is categorized as gradient-based nonlinear programming. The sensitivity coefficients are computed using a finite difference approach. The member with $B_i = 0.01$ in the optimal solution is regarded as an unnecessary member to be removed. Since the problem is highly nonlinear, the solutions are obtained from randomly generated five different initial solutions. The optimal solutions Opt1, ..., Opt5 are shown in Fig. 17, where the thickness of each member is proportional to its size B_i.

Note that Opt5 has floating members, because the structural volume is not minimized in the process of optimization. By contrast, Opt1, Opt2, and Opt3 manifest how horizontal and vertical loads are transmitted to the supports through the flexible base. Opt2 and Opt3 have stiff base beam as assemblage of frame elements, which is supported by a vertical member at the center and the diagonal members at both sides.

Figure 18 shows the trajectory between the rocking angle and net drift angle of Opt1 for the seismic motion in Fig. 5(b). From the figure, we can confirm rocking of the base in the opposite direction to the drift of the upper frame, which leads to reduction of the roof displacement.

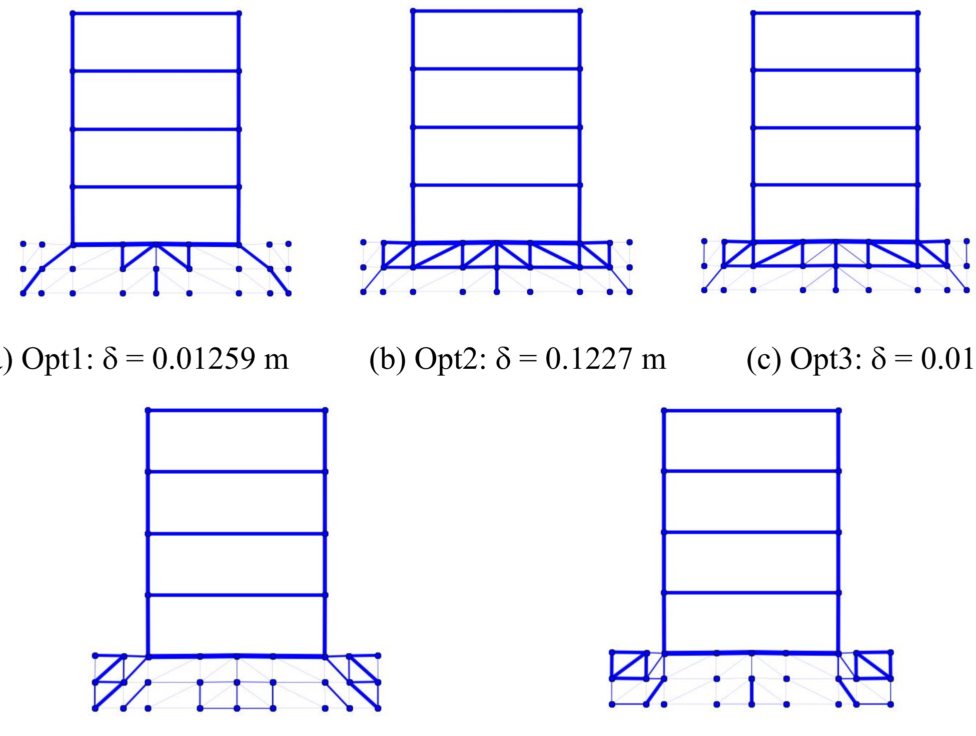

(a) Opt1: δ = 0.01259 m (b) Opt2: δ = 0.1227 m (c) Opt3: δ = 0.01228 m

(d) Opt4: δ = 0.01302 m (e) Opt5: δ = 0.01292 m

Fig. 17. Optimal solutions of the frame model Opt1, …, Opt5 obtained from randomly generated different initial solutions; thickness of each member is proportional to its cross-sectional size B_i, and the member with $B_i = 0.01$ is removed.

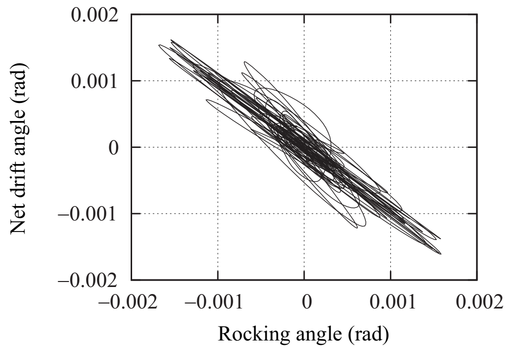

Fig. 18. Trajectory of rocking angle and drift angle of Opt1 subjected to the seismic motion in Fig. 5(b).

6. Conclusion

Reverse rocking response under seismic motion has been investigated for a steel frame that has flexible base. A condition for reverse rocking response has been derived using a simple model. An optimization approach has also been proposed for design of flexible base for seismic response reduction of building frames. The conclusions drawn from this study are summarized as follows:

1. The displacement as well as acceleration of the roof of a frame under seismic ground motion can be effectively reduced using a flexible base structure, which utilizes rocking of the base in the opposite direction to the drift of the upper frame. Such reverse rocking response is dominated by the 2nd mode rather than the 1st mode.
2. The large horizontal displacement at a roller support of the flexible base can be effectively utilized to install viscous dampers for further reduction of seismic responses.
3. Various types of flexible base consisting of frame members can be generated through optimization under constraints on roof displacement and 1st natural frequency. It is also effective to assign constraints on the participation factors for the 1st and 2nd modes to ensure dominance of the 2nd mode to enhance rocking response of the base in the opposite direction to the drift of the upper frame. The mean maximum roof displacement, which is computed using the SRSS method, is minimized as the objective function. Optimal cross-sectional sizes and geometrical properties can be found by a random start nonlinear programming.

References

1. Meek JW. Effects of foundation tipping on dynamic response. J Struct Div, ASCE 1975;101(7):1297-1311.
2. Ishihara T, Azuhata T, Midorikawa M. Modal analysis of dynamic behavior of buildings allowed to uplift at mid-story. Proc. 15th World Conf. on Earthquake Eng., Lisbon, Portugal, 2012; Paper ID:4635.
3. Azuhata T, Ishihara T, Midorikawa M. Multi-dimensional earthquake response of self-centering building structural system using uplift mechanism, Proc. 15th World Conf. on Earthquake Eng., Lisbon, Portugal, 2012; Paper ID: 1960.
4. Gelagoti F, Kourkoulis R, Anastasopolous A, Gazetas G. Rocking isolation of low-rise frame structures founded on isolated footings. Earthquake Eng Struct Dyn 2012; 41: 1177-1197.
5. Deierlein G, Krawinkler H, Ma X, Eatherton M, Hajjar J, Takeuchi T, Kasai K, Midorikawa M. Earthquake resilient steel braced frames with controlled rocking and energy dissipating fuses. Steel Construction; 2011: 4(3): 171-175.
6. Midorikawa M, Azuhata T, Ishihara T, Wada A. Shaking table tests on seismic response of steel braced frames with column uplift. Earthquake Eng Struct Dyn; 2006: 35: 1767-1785.
7. Midorikawa M, Takeuchi T, Hikino T, Kasai K, Deierlein G, Oobayashi M, Yamazaki R, Kishiki S. Seismic performance of controlled rocking frames with shear fuse and PT wire anchorage, Part 1: Shaking table tests on controlled rocking steel frames using multipurpose inertial mass system. J Struct Constr Eng, Architectural Inst. Japan 2010; 75(654): 1547-1556. (in Japanese)
8. Fakhouri MY, Igarashi A. Multiple-slider surfaces bearing for seismic retrofitting of frame structures with soft first stories. Earthquake Eng Struct Dyn; 2013: 42: 145-161.
9. Briman V, Ribakov Y. Using seismic isolation columns for retrofitting buildings with soft stories, The Structural Design of Tall and Special Buildings; 2009: 18: 507-523.
10. Hwasung R, Reinhorn AM. Modeling and seismic response of structures with

concrete rocking columns and viscous dampers. Engineering Structures 2010; 32(8): 2096-2107.

11. Lu LY, Hsu CC. Experimental study of variable-frequency rocking bearings for near-fault seismic isolation. Engineering Structures 2013; 46: 116-129.
12. Howell LL, Compliant mechanisms. Wiley; 2001.
13. Sigmund O. On the design of compliant mechanisms using topology optimization. Mech Struct & Mach 1997; 25(4): 493-524.
14. Ohsaki M, Nishiwaki S. Shape design of pin-jointed multistable compliant mechanism using snapthrough behavior. Struct Multidisc Optim 2005; 30: 327-334.
15. Kinoshita T, Ohsaki M. Shape optimization of compliant mechanisms for seismic isolator model. Journal of Structural and Constructional Engineering 2010; 75(647): 113-119. (in Japanese)
16. Kinoshita T, Ohsaki M, Nakajima T. Topology optimization of compliant mechanisms for vertical seismic isolation of spatial structures. J Int Assoc for Shell and Spatial Struct 2009; 50(2): 89-96.
17. Tsuda S, Ohsaki M. Parameter optimization of mass damper consisting of compliant mechanism for bi-directional control of spatial structures. J Struct Constr Eng, Architectural Inst. Japan 2013; 77(673): 379-387. (in Japanese)
18. Tsuda S, Ohsaki M. Bi-directional seismic vibration control of spatial structures using passive mass damper consisting of compliant mechanism. Proc. IASS-APCS Symp. 2012, Seoul: Paper No. 109.
19. Nakamura T, Ohsaki M. Sequential generator of earthquake-response constrained trusses for design strain ranges. Comput & Struct 1989; 33(6): 1403-1416.
20. Ohsaki M, Nakamura T, Isshiki Y. Shape-size optimization of plane trusses with designer's preference. J Struct Engng, ASCE 1998; 124(11): 1323-1330.
21. Takezawa A, Kitamura M. Sensitivity analysis and optimization of vibration modes in continuum systems. J Sound Vib 2013; 332: 1553-1566.
22. Tsai TD, Cheng CC. Structural design for desired eigenfrequencies and mode shapes using topology optimization. Struct Multidisc Optim 2013; 47: 673-686.
23. Todorovska MI. Base isolation by a soft first story with inclined columns. J Eng Mech 1999; 125: 448-457.

24. Zhang F. Vibration control of buildings by connecting different stories using rocking and lever mechanism. J Struct Constr Eng, Architectural Inst. Japan 2006; 599: 35-42. (in Japanese)
25. Zhang F. Rocking center designated mechanism and structure control. J Struct Constr Eng, Architectural Inst. Japan 2001;544:53-60. (in Japanese)
26. Chen YH, Liao WH, Lee CL, Wang YP. Seismic isolation of viaduct piers by means of a rocking mechanism. Earthquake Eng Struct Dyn 2006; 35: 713-736.
27. Pollino M, Bruneau M. Dynamic seismic response of controlled rocking bridge steel-truss piers. Engineering Structures 2008; 30(6): 1667-1676.
28. Scanlan RH, Sachs K. Earthquake rime histories and response spectra. J Eng Mech Div, ASCE 1974; EM4: 635-655.
29. Iyenger RN, Rao PN. Generation of spectrum compatible accelerograms. Earthquake Eng Struct Dyn 1979; 7: 253-263.
30. Ohsaki Y. On the significance of phase content in earthquake ground motions. Earthquake Eng Struct Dyn 1979; 7: 427-439.
31. Open System for Earthquake Engineering Simulation (OpenSees), PEERC, UC Berkeley. http://opensees.berkeley.edu/, Nov. 7, 2013.
32. Ohsaki M, Nakajima T, Fujiwara J, Takeda F. Configuration optimization of clamping members of frame-supported membrane structures, Engineering Structures 2011; 33: 3620-3627.
33. Gill PE, Murray W, Saunders MA. SNOPT: An SQP algorithm for large-scale constrained optimization. SIAM J Opt 2002; 12: 979-1006.